

# Assessing the quantitative reliability of solid-state $^{13}\text{C}$ NMR spectra of kerogens across a gradient of thermal maturity

Ronald J. Smernik<sup>a,\*</sup>, Lorenz Schwark<sup>b</sup>, Michael W.I. Schmidt<sup>c</sup>

<sup>a</sup>*Soil and Land Systems, School of Earth and Environmental Sciences, The University of Adelaide, Waite Campus, Urrbrae, SA 5064, Australia*

<sup>b</sup>*Geological Institute, Cologne University, Zulpicher Str. 49a, D-50674, Cologne, Germany*

<sup>c</sup>*Department of Geography, University of Zürich, 8057 Zürich, Germany*

Received 15 September 2005; received in revised form 24 October 2005

Available online 28 November 2005

## Abstract

Five type II kerogens, shown by elemental analysis and Rock-Eval pyrolysis to represent a gradient of thermal maturity, were further characterized using a range of solid-state  $^{13}\text{C}$  NMR spectroscopic techniques.  $^{13}\text{C}$  cross polarization (CP) NMR spectra of the kerogens confirmed the well-established pattern of increasing aromaticity with increasing thermal maturity. Spin counting showed that CP observability was around 50% for the immature kerogens, and only 14–25% for the mature kerogens. Spin counting also showed that the direct polarization (DP) observabilities were >80% for all but one of the kerogens. Despite the large differences in observability between the two techniques, aromaticities derived from corresponding CP and DP spectra differed by only 1–15%. The RESTORE technique showed that the low CP observability of the immature kerogens was due mostly to rapid  $T_{1\rho}H$  relaxation, whereas both rapid  $T_{1\rho}H$  relaxation and slow polarization transfer contributed to the low CP observability of the mature kerogens.

© 2005 Elsevier Inc. All rights reserved.

**Keywords:** Solid-state  $^{13}\text{C}$  NMR; Kerogen; Quantitation; Spin counting; RESTORE

## 1. Introduction

Kerogen is the insoluble organic matter found in sedimentary rocks and is derived from organic remains laid down in sediments [1]. It is of great economic importance, as geothermal heating effects chemical changes to kerogen that result in the generation of oil and gas. Kerogen is also of importance in other scientific spheres. Kerogen is the largest reservoir of organic C on earth [2], and is thus a key component of the global C cycle. The amount of C stored in sedimentary rocks has a dominant effect on the atmospheric  $\text{O}_2$  concentration on the geological timescale [3]. Kerogen has also been identified as an important high-affinity sorbate for hydrophobic organic contaminants [4–8].

All of these properties of kerogen (oil and gas potential, effect on the global C cycle and HOC sorption) are a function of its chemical structure, which in turn is

dependent on its paleoenvironmental origin and the degree to which it has already been transformed (i.e. its thermal maturity). Kerogens can be divided into three main types based on differences in paleoenvironmental origin [1]. Type I kerogens are typically derived from lacustrine environments and consist mainly of saturated hydrocarbon-rich algal remains. Type II kerogens are typically derived from marine sediments, whilst type III kerogens have a predominantly terrestrial plant origin. These differences result in different chemical compositions of thermally immature kerogens of the different types. For example, immature type I kerogens typically have the highest H/C ratios, whilst immature type III kerogens have the highest O/C ratios. The process of thermal maturation decreases first O/C, then H/C ratios [1,9,10]. With increasing thermal maturity, differences in chemical composition between the three kerogen types become less prominent as they all trend towards unfunctionalized, condensed aromatic structures [1,10].

Solid-state  $^{13}\text{C}$  NMR spectroscopy has proven to be a very useful technique for detecting differences in kerogen

\*Corresponding author. Fax: +61 8 8303 6511.

E-mail address: [ronald.smernik@adelaide.edu.au](mailto:ronald.smernik@adelaide.edu.au) (R.J. Smernik).

composition, both in terms of paleoenvironmental origin and maturity [9–24]. Immature type I kerogens are very rich in long-chain alkyl C [14,17,19,23], whilst immature type III kerogens contain substantial amounts of *O*-alkyl and *O*-aryl functional groups [17]. Increasing maturity results first in the loss of oxygen functionalities (if present), followed by increasing aromaticity [9–12,16,21,24] and increased condensation of aromatic structures [9,10,24].

To date, most solid-state  $^{13}\text{C}$  NMR studies of kerogen have involved quantifying signal in a range of chemical shift regions and assigning these to specific functional groups. There is an inherent danger in this approach, due to the fact that the NMR signal of some functional groups can be compromised, especially when the cross polarization (CP) technique is used. This issue has been discussed widely in the coal literature [25], and has led to the greater use of the more quantitatively reliable direct polarization (DP) technique [26], otherwise known as Bloch decay or single pulse excitation. The quantitative reliability of  $^{13}\text{C}$  CP NMR analyses of kerogens has also been discussed [10,14,17,20,22,24], but CP is still the most widely used technique [10,21–24]. Few DP spectra of kerogen have been presented [10,22]. We have found a simple calibration procedure called spin counting to be very useful for diagnosing NMR quantitation problems in the analysis of organic matter derived from soils [27,28] and sediments [29]. There is a long history of the use of spin counting in NMR studies of coals [25,30–35], but the technique has rarely been applied to kerogens [22]. We have also developed a technique called RESTORE that can identify the cause of poor quantitation in  $^{13}\text{C}$  CP NMR spectra [36].

In this paper, we assess the quantitative reliability of solid-state  $^{13}\text{C}$  NMR spectra of a range of kerogens of similar paleoenvironmental origin (type II kerogens) across a gradient of thermal maturity. The aim is to determine whether some kerogens are poorly seen by NMR, and if so, why, and more broadly to provide an objective basis on which to judge the quantitative reliability of NMR analyses of kerogens.

## 2. Materials and methods

### 2.1. Collection and description of shale samples

Kerogens analyzed in this study originate from four Upper Permian (Kupferschiefer/Marl Slate and Irati Shale) and one Lower Jurassic (Posidonia Shale) organic matter rich rocks deposited in continental shelf areas (Table 1).

The Posidonia Shale, from which kerogen 1 was isolated, is a transgressive black shale of Lower Toarcian age (183 Ma) with considerable carbonate content due to accumulation of coccolithophoroid shells. Deposition took place under intensive stratification with strongly reducing bottom waters underlying a low-salinity surface water lens derived from continental freshwater run-off [37]. Organic matter is of marine algal and bacterial origin representing a typical type II kerogen and is close to reaching the onset of the oil window.

The Kupferschiefer, which covers an area of  $>600,000\text{ km}^2$ , is a transgressive black shale deposited under reducing conditions immediately after the flooding of the Central European Zechstein Basin (251 Ma). Two Kupferschiefer samples originate from the Lower Rhine Embayment (LRE), where the thermal maturity of the organic matter has not yet reached the oil window. The sediment is developed in a marginal facies type, characterized by dilution of organic and siliciclastic matter by carbonate precipitation [38]. The organic matter is of type II kerogen for the basal Kupferschiefer (kerogen 2) and type II kerogen with admixture of type III kerogen for the upper regressive part of the Kupferschiefer (kerogen 3). Carbonate-poor basinal Kupferschiefer forms a thin layer of only 20–30 cm thickness characterized by a uniform organic facies of marine type II kerogen. Kerogen 4 from well Goslar Z6, drilled NW of the Hercynian mountains [39], represents basinal Kupferschiefer with organic matter in the maturity range of the late oil window.

Replicate samples of kerogens 3 and 4 (labeled kerogen 3a and kerogen 4a) were prepared to gauge the accuracy of some of the analyses. Replicate kerogen pairs 3 and 3a,

Table 1  
Kerogen source, age and yields, and elemental analyses of shales and kerogens

	Formation	Stratigraphic age	Yield ( $\text{mg g}^{-1}$ )	Elemental analyses						
				C			H			Kerogen H/C ratio
				Shale ( $\text{mg g}^{-1}$ )	Kerogen ( $\text{mg g}^{-1}$ )	Recovery (%)	Shale ( $\text{mg g}^{-1}$ )	Kerogen ( $\text{mg g}^{-1}$ )	Recovery (%)	
Kerogen 1	Posidonia shale	Jurassic	268	143	503	94	20.5	47.3	62	.094
Kerogen 2	Kupferschiefer	Permian	193	73	478	126	12.4	36.5	57	.076
Kerogen 3	Kupferschiefer	Permian	187	30	154	96	9.7	13.8	27	.090
Kerogen 3a	Kupferschiefer	Permian	154	31	173	86	9.4	16.3	27	.094
Kerogen 4	Kupferschiefer	Permian	314	221	618	88	15.3	29.1	60	.047
Kerogen 4a	Kupferschiefer	Permian	317	224	613	87	14.9	28.1	60	.046
Kerogen 5	Irati shale	Permian	25	18	583	82	9.8	16.8	4	.029

and 4 and 4a were prepared from subsamples of a single batch of the corresponding shales.

The Upper Permian Irati Shale is time-equivalent to the Kupferschiefer samples and consists of organic-rich shales, marls and limestones deposited on a shelf with restricted water circulation and establishment of strongly reducing conditions. Kerogen 5 represents Irati Shale in the carbonate facies of the Middle Assistencia Formation, with a thermal maturity corresponding to the late oil window [40]. The Irati Shale carbonate sample contained some allochthonous bitumen of lower thermal maturity than the indigenous kerogen. These impregnating fluids were removed during kerogen isolation.

### 2.2. Kerogen isolation

Sediment samples were cleaned on the outside, crushed and ground to analytical grain size ( $<0.2$  mm) and then extracted with organic solvents to remove bitumen. Extraction was carried out by accelerated solvent extraction using dichloromethane under conditions as outlined in [41]. Carbonate was removed by treatment of sediment, first with 10% hydrochloric acid until  $\text{CO}_2$  evolution ceased, then followed by treatment with 25% hydrochloric acid. Decalcified samples were washed with deionized water until neutral and dried at  $80^\circ\text{C}$  for 12 h.

Hydrofluoric acid (40%, 25 mL) was added to aliquots of the decalcified shale (1 g) in plastic centrifuge tubes. After the reaction subsided, the tubes were placed in a  $50^\circ\text{C}$  water bath and stirred once an hour for 8 h. The tubes were removed from the water bath and stored at room temperature overnight. The next day, further HF was added (40%, 10 mL) and the tubes were placed in a  $70^\circ\text{C}$  water bath and stirred once an hour for 8 h. The samples were cooled to room temperature, water (35 mL) was added, and the tubes were centrifuged at 4000 rpm for 7 min. The supernatant was discarded and the washing procedure was repeated twice more with water (35 mL). Hydrochloric acid (32%, 10 mL) was added to the residue and the tubes were heated at  $50^\circ\text{C}$  for 1 h in order to remove fluoride precipitates. The residue was isolated by centrifugation and the procedure repeated until the supernatant remained colorless. Finally, the residue was rinsed six times with water (20 mL), then oven-dried overnight at  $130^\circ\text{C}$ . Kerogen yields and elemental analyses are reported in Table 1. Carbon recoveries on kerogen isolation (Table 1) ranged from 82% to 96%, except for kerogen 2, for which the anomalous value of 126% probably reflects differences in C content between aliquots used for whole shale C determination and kerogen isolation.

### 2.3. Elemental analysis

Carbon and nitrogen concentrations were determined on an Elementar Vario EL analyzer.

### 2.4. Rock-Eval analysis

Sediment samples were subjected to Rock-Eval pyrolysis following standard procedures [42,43]. About 60 mg of bulk, dried sample was weighed into stainless steel crucibles equipped with platinum mesh lids and heads to allow through flow of carrier gas. Samples were heated in an inert helium atmosphere. Following thermo-vaporization and pyrolysis, hydrocarbons were quantified by flame-ionization detection. Compounds occurring as free gases and liquids in sediments were separated from those that occur in bound form or constitute the kerogen by temperature control. The S1-detector signal records free bitumen, which is thermo-vaporizable at  $300^\circ\text{C}$ . Since the samples studied here were pre-extracted with organic solvents, they only yielded minor S1 signals.

The S2-detector signal measures those compounds liberated from the kerogen during programmed pyrolysis from 300 to  $550^\circ\text{C}$ . The amount of hydrocarbons generated during pyrolysis normalized to the amount of organic carbon comprises the hydrogen index (HI). The temperature of maximum S2-pyrolysate yield is recorded as  $T_{\text{max}}$  and provides an estimate of the thermal maturity of the kerogen. The ratio of  $S1/(S1+S2)$  is termed the production index (PI) and refers to the percentage of potentially convertible organic matter that has been released from the kerogen. The PI was very low for the samples studied here due to solvent pre-extraction.

In addition to the determination of hydrogen richness of kerogen, its oxygen content is assessed by measuring the  $\text{CO}_2$  generated from the organic matter between 300 and  $390^\circ\text{C}$ .  $\text{CO}_2$  released at higher temperatures may derive from carbonate dissociation and is ignored in the estimation of organic matter oxygen content. Pyrolytic  $\text{CO}_2$  normalized to organic carbon yields the oxygen index (OI). Upon increasing thermal maturation, both the HI and the OI values of kerogen decrease.

### 2.5. NMR spectroscopy

Solid-state  $^{13}\text{C}$  magic angle spinning (MAS) NMR spectra were obtained at a  $^{13}\text{C}$  frequency of 50.3 MHz on a Varian Unity200 spectrometer. Samples were packed in a 7 mm diameter cylindrical zirconia rotor with Kel-F end-caps and spun at  $5000 \pm 100$  Hz in a Doty Scientific MAS probe. CP spectra were acquired using a 1-ms contact time and a 0.5-s recycle delay; 10,000 scans were collected for each spectrum, except for kerogen 5 (100,000 scans collected). DP spectra were acquired using a 6.0-ms ( $90^\circ$ )  $^{13}\text{C}$  pulse. A recycle delay of 90 s was used for all samples and 1000 transients were collected for each sample. DP spectra were corrected for background signal [44]. Free induction decays for both CP and DP spectra were acquired with a sweep width of 40 kHz; 1216 data points were collected over an acquisition time of 15 ms. All spectra were zero-filled to 8192 data points and processed with a

50-Hz Lorentzian line broadening and a 0.005-s Gaussian broadening. Chemical shifts were externally referenced to the methyl resonance of hexamethylbenzene at 17.36 ppm.

Spin counting experiments were performed using the method of Smernik and Oades [27,45]. Glycine (AR grade, Ajax Chemicals) was used as an external intensity standard (i.e. the glycine spectrum was acquired separately to those of the samples). For CP spin counting experiments, differences in spin dynamics between the sample and the glycine standard were accounted for using the method of Smernik and Oades [45], except that a variable spin lock (VSL) rather than a variable contact time (VCT) experiment was used to determine  $T_{1\rho}H$  [46]. Errors in carbon NMR observabilities ( $C_{\text{obs}}$  values) are estimated to be  $\pm 10\%$  in  $C_{\text{obs}}\text{--CP}$  and  $\pm 15\%$  in  $C_{\text{obs}}\text{--DP}$  [45].

VCT and VSL experiments were performed as part of the RESTORE procedure [36] for determining rates of  $T_{1\rho}H$  relaxation and rates of polarization transfer ( $T_{\text{CH}}$ ). VCT experiments consisted of an array of eight contact times (2, 2.5, 3, 4, 5, 6, 8, 10 ms). The experiments were run in an interleaved fashion, with 32 scans acquired for each contact time, in turn. This was repeated until a total of 4000 scans was acquired. A 0.5-s recycle delay was employed for all samples.

VSL experiments were performed with three different contact times, 200  $\mu\text{s}$ , 1 and 2 ms. For the 200- $\mu\text{s}$  contact time VSL experiments, ten spin lock times were used (0, 0.3, 0.8, 1.3, 1.8, 2.3, 2.8, 3.8, 4.8 and 5.8 ms), for the 1-ms contact time VSL experiments, ten spin lock times were used (0, 0.5, 1, 1.5, 2, 3, 4, 5, 7 and 9 ms) and for the 2-ms contact time VSL experiments, eight spin lock times were used (0, 0.5, 1, 2, 3, 4, 6 and 8 ms). The VSL experiments were run in an interleaved fashion, with blocks of 32 scans acquired in turn, to a total of 4000, with a 0.5-s recycle delay between scans.

Three spectra were acquired as input spectra for generating RESTORE subspectra; a 1-ms contact time—0 spin lock spectrum, a 5- or 6-ms contact time—0 spin lock spectrum, and a 1-ms contact time—1-, 2- or 3-ms spin lock spectrum. These spectra were acquired in an interleaved fashion, with blocks of 32 scans acquired in turn, to a total of 10,000–25,000, with a 0.5-s recycle delay between scans.

### 3. Results and discussion

#### 3.1. Characterization of kerogen by elemental and Rock-Eval analysis

The Posidonia Shale sample (kerogen 1) was shown by elemental and Rock-Eval analysis to be an algal-derived marine kerogen of a moderate maturity corresponding to a vitrinite reflectivity of about 0.5% Rr. This is in excellent agreement with previous paleocological, organic and isotope geochemical studies [37,47–51]. The PI ratio of less than 0.02 (Table 2) confirms that the kerogen concentrate is devoid of impregnating bitumen that may eventually affect NMR analysis.

The Kupferschiefer samples clearly separate into thermally mature samples from well Goslar Z6 (kerogens 4 and 4a) and immature samples from the LRE (kerogens 2, 3 and 3a). For samples from the Zechstein Dolomite, which is nearly time-equivalent to the Kupferschiefer and contains marine type II kerogen, Vliex et al. [39] obtained vitrinite reflectivities of approximately 0.82% Rr. This is in good agreement with the  $T_{\text{max}}$  and HI values determined on kerogens 2, 3 and 3a (Table 2). The low-maturity LRE samples show a differentiation according to the amount of admixed terrigenous organic matter. Kerogen 2, which is from the basal part where organic matter is almost exclusively of algal marine type II kerogen, shows a HI value of 380 mgHC/gTOC, whereas kerogens 3 and 3a, which are affected by minor admixture of terrigenous organic matter yield HI values of 322–327 mgHC/gTOC (Table 2). The H/C ratio of the LRE kerogens agree reasonably well with the HI values. However, the more terrigenous and thus hydrocarbon-depleted kerogens 3 and 3a cannot be differentiated from the fully marine type II kerogen 2 on the basis of their H/C ratios (Table 1). The low carbon concentrations ( $<200 \text{ mg g}^{-1}$ ) of kerogens 3 and 3a (Table 1) can be attributed to the high abundance of pyrite in these samples.

The Assistencia Member sample (kerogen 5) was isolated from the organic matter lean facies variety of the Irati Shale. Although the TOC concentration of the sediment was very low for this sample (Table 1), the isolated kerogen has a very high TOC concentration ( $583 \text{ mg g}^{-1}$ ). The high carbon concentration is accompanied by a low H/C ratio

Table 2  
Results from Rock-Eval analyses

	$T_{\text{max}}$ (°C)	$S_1$ ( $\text{mg g}^{-1}$ )	$S_2$ ( $\text{mg g}^{-1}$ )	$S_3$ ( $\text{mg g}^{-1}$ )	HI	OI	PI
Kerogen 1	428 (3)	5.62 (0.85)	311 (30)	6.6 (3.3)	618	13	0.02
Kerogen 2	423 (2)	3.68 (0.51)	182 (14)	13.3 (8.7)	380	28	0.02
Kerogen 3	427 (3)	1.41 (0.16)	50.4 (4.3)	4.5 (1.1)	327	29	0.03
Kerogen 3a	424 (2)	1.48 (0.14)	55.7 (2.7)	6.3 (2.2)	322	37	0.03
Kerogen 4	450 (6)	1.45 (0.20)	16.9 (2.0)	2.9 (1.4)	27	5	0.08
Kerogen 4a	454 (1)	2.03 (0.25)	17.1 (2.4)	3.5 (0.6)	28	6	0.11
Kerogen 5	405 (—)	1.33 (—)	7.0 (—)	3.2 (—)	12	5	0.16

and HI value (Tables 1 and 2). This points towards a highly mature organic matter composition, which is not reflected by the low  $T_{\max}$  value, due to a low S2 yield (Table 2). Most of the carbon of kerogen 5 is thus refractory and not accessible to Rock-Eval analysis. The maturity of the kerogen is estimated to be  $>0.9\%$  Rr. A precise determination of maturity is impossible due to the lack of vitrinites in the sample and the fact that biomarker maturity parameters are not applicable based on the presence of impregnating bitumens.

### 3.2. Comparison of $^{13}\text{C}$ CP and DP NMR spectra

The  $^{13}\text{C}$  CP and DP spectra of the five kerogens are shown in Fig. 1. The NMR spectra fall into two groups. The spectra of kerogens 1–3 are dominated by two broad resonances, one in the alkyl C region centred at 30–31 ppm and one in the aromatic region centred at 128–132 ppm. For each kerogen, the aromatic resonance is slightly stronger in the DP spectrum compared to the corresponding CP spectrum. These spectra are similar to previously published NMR spectra of type II kerogens of low thermal

Table 3  
Assignment of chemical shift regions

Region	Assignment
A: 260–190 ppm	Aromatic SSB
B: 190–160 ppm	Carbonyl
C: 160–90 ppm	Aromatic center band
D: 90–10 ppm	Aliphatic + aromatic SSB
Carbon type	Region/combination of regions
Carbonyl	B
Aromatic	C + 2 × A
Aliphatic	D–A

maturity [10,18]. The spectra of kerogen samples 4 and 5 are dominated by a resonance in the aromatic region. This resonance is centred at 127–128 ppm for kerogen 4 and at 124–125 ppm for kerogen 5. Small resonances in the alkyl region are also evident in the spectra of kerogens 4 and 5, although these overlap with the spinning sidebands (SSBs) of the aromatic resonance. Once again, these spectra are similar to previously published NMR spectra of type II kerogens of high thermal maturity [10].

The distribution of signal in each of the spectra was quantified by integrating the spectral intensity over the chemical shift ranges defined in Table 3. SSBs were corrected for by assuming that the high-field and low-field SSBs were of equal intensity. Although this is not necessarily true, we show below that the high-field and low-field SSBs for kerogens 4 and 5 appear to be of similar magnitude. The intensity of the low-field SSB of the aromatic resonance was 7–12% of the aromatic centre band for all of the kerogen spectra.

Table 4 shows that the kerogen aromaticities determined from the  $^{13}\text{C}$  CP NMR spectra ranged from 31.1% to 45.2% for the thermally immature kerogens 1–3, and from 80.6% to 83.0% for the thermally mature kerogens 4 and 5. The partial terrigenous source of kerogen 3 is reflected in its greater aromaticity relative to kerogen 2, which is of similar maturity, but is fully marine. The proportion of aromatic carbon correlates inversely with the Rock-Eval HI index (Fig. 2), a finding consistent with previous studies [9,16–18,24].

Aromaticities determined from the DP spectrum were 1–15% higher than those determined from the CP spectrum for each kerogen (Table 4). This is consistent with the findings of Werner-Zwanziger et al. [10].

### 3.3. Spin counting

Results of spin counting on the  $^{13}\text{C}$  CP and DP spectra of the kerogens are reported in Table 5. The first point to note is that the proportion of potential NMR signal detected in the DP spectra ( $C_{\text{obs}} - \text{DP}$ ) was higher than in the corresponding CP spectra ( $C_{\text{obs}} - \text{CP}$ ) by at least 50%, and up to a factor of almost four. The  $C_{\text{obs}} - \text{DP}$  values for kerogens 1–4 of 84–88% indicate that nearly all potential

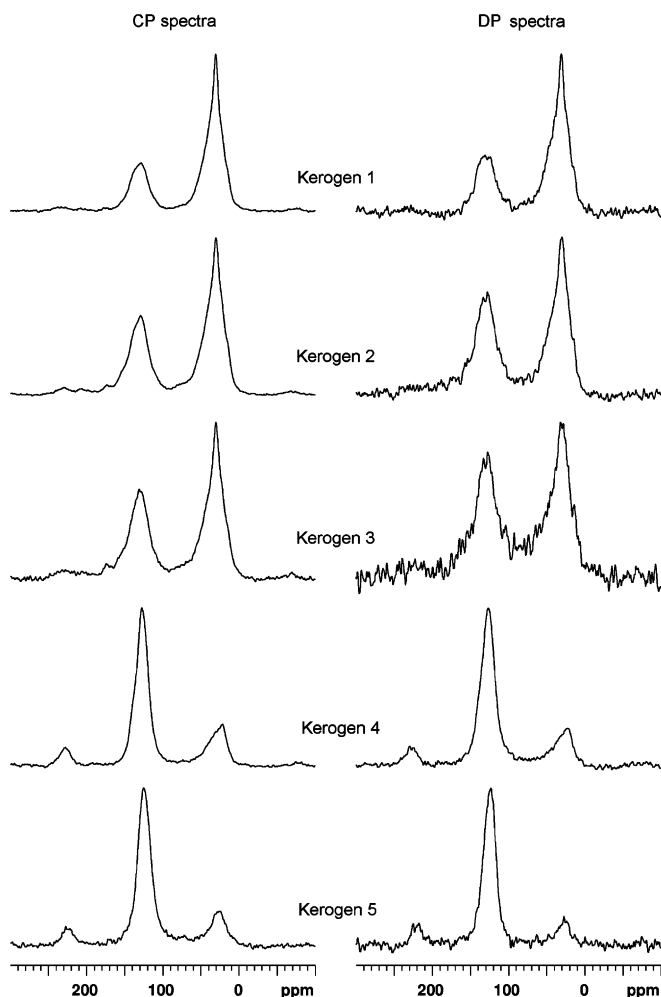


Fig. 1. Solid-state  $^{13}\text{C}$  CP and DP spectra of the kerogens.

Table 4  
Percentage of total signal assigned to three carbon types for  $^{13}\text{C}$  CP and DP NMR spectra of the kerogens

	Carbonyl		Aromatic		Aliphatic	
	CP	DP	CP	DP	CP	DP
Kerogen 1	1.0	0.2	31.1	34.8	68.0	64.9
Kerogen 2	2.6	4.2	40.8	46.8	56.6	49.0
Kerogen 3	3.6	4.0	45.2	47.7	51.2	48.3
Kerogen 4	0.6	1.7	80.6	81.3	18.7	17.0
Kerogen 5	1.8	2.0	83.0	89.9	15.2	8.1

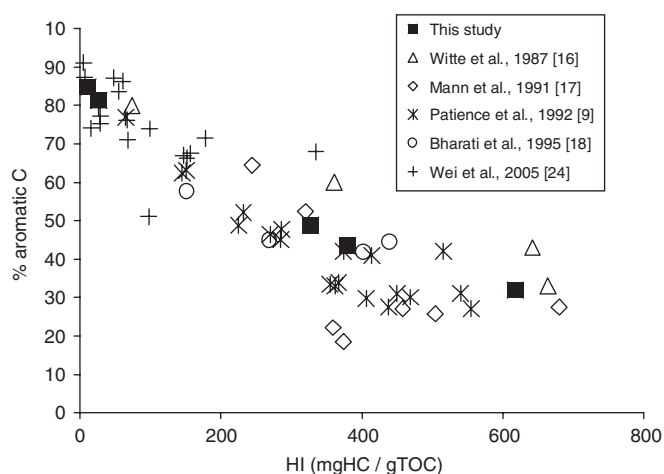


Fig. 2. Plot of kerogen aromaticity versus Rock-Eval HI index for kerogens 1–5, in comparison with previous studies.

Table 5  
Results of spin counting— $^{13}\text{C}$  NMR observabilities for CP ( $C_{\text{obs-CP}}$ ) and DP ( $C_{\text{obs-DP}}$ ) spectra

	$C_{\text{obs-CP}}$ (%)	$C_{\text{obs-DP}}$ (%)
Kerogen 1	50	84
Kerogen 2	57	84
Kerogen 3	48	88
Kerogen 4	25	85
Kerogen 5	14	59

signal was detected, and that therefore the signal distribution in these DP spectra is quantitatively reliable. The  $C_{\text{obs-DP}}$  value for kerogen 5 was substantially lower at 59%. The  $C_{\text{obs-CP}}$  values were much higher for the less mature kerogens 1–3 (48–57%) than for the more mature kerogens 4–5 (14–25%).

Combining the spin counting and spectral distribution information provides some interesting insights. As discussed above, comparison of corresponding CP and DP spectra for kerogens 1–3 indicates that aromaticity is under-represented by around 10% in the CP spectra. However, the differences in CP and DP observabilities are much greater than this. Clearly, the ~50% of potential signal not detected by CP for these kerogens cannot all be

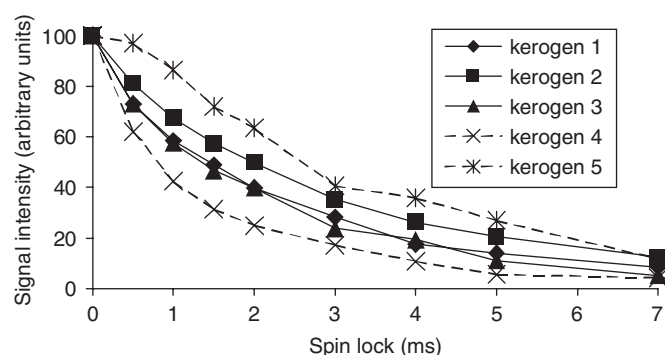


Fig. 3. Plots of signal intensity versus  $^1\text{H}$  spin lock for VSL experiments on the kerogens. Data for the three thermally immature kerogens are plotted with an unbroken line; data for the two thermally mature kerogens are plotted with a broken line.

aromatic C. Furthermore, not all aromatic C are detected with equal efficiency. Both kerogens 4 and 5 are predominantly aromatic, yet both  $C_{\text{obs-CP}}$  and  $C_{\text{obs-DP}}$  are 30–45% lower for kerogen 5.

### 3.4. RESTORE

There are two mechanisms that cause inefficient detection of CP NMR signal: (i) slow transfer of  $^1\text{H}$  magnetization to  $^{13}\text{C}$  nuclei during the contact time, and (ii) rapid decay of magnetization (especially of  $^1\text{H}$  nuclei) during the contact time. The rate of decay of  $^1\text{H}$  magnetization during the contact time ( $T_{1\rho}H$ ) was determined using the VSL experiment [46]. Fig. 3 shows that  $T_{1\rho}H$  relaxation rates were very similar for kerogens 1 and 3, and similar, though slightly slower for kerogen 2. On the other hand,  $T_{1\rho}H$  relaxation rates for the two thermally mature kerogens were very different, with kerogen 4 having the most rapid  $T_{1\rho}H$  relaxation rate and kerogen 5 the slowest. Signal decay is significantly non-exponential for kerogens 1–4, with rates of decay more rapid at shorter spin lock times (see below). This indicates the presence of a rapidly relaxing component in kerogens 1–4, which is under-represented in the normal CP spectra.

The presence of  $^{13}\text{C}$  nuclei that cross polarize slowly can be detected by comparing signal intensity in VSL and VCT experiments. In a VCT experiment, signal intensity is a

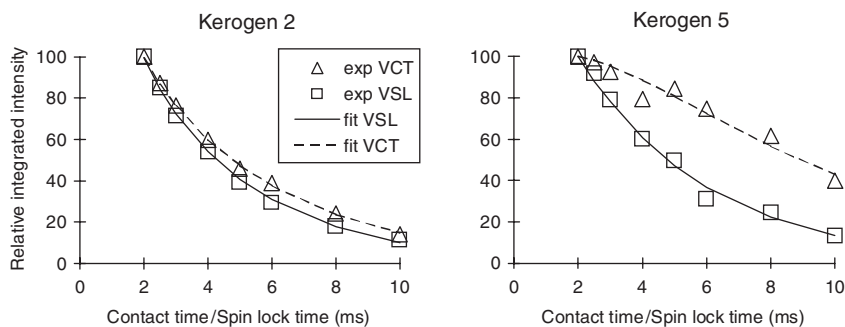


Fig. 4. Plots of signal intensity versus  $^1\text{H}$  spin lock/contact time for VSL/VCT experiments on kerogens 2 and 5.

function of both the rate of polarization transfer ( $T_{\text{CH}}$ ) and the rate of  $T_{1\rho}H$  relaxation. In a VSL experiment, signal intensity is a function of the rate of  $T_{1\rho}H$  relaxation only. Fig. 4 shows that VCT intensities are slightly higher than VSL intensities for kerogen 2, indicating that there is a small amount of polarization transfer occurring at contact times greater than 2 ms. However, for kerogen 5 (Fig. 4), VCT intensities are much higher than VSL intensities, indicating that there is substantial polarization transfer occurring at contact times greater than 2 ms.

The RESTORE (*RE*storation of Spectra via  $T_{\text{CH}}$  and *T* One Rho ( $T_{1\rho}H$ ) Editing) technique [36] enables quantification of the effects of rapid  $T_{1\rho}H$  relaxation and slow polarization transfer. The basic concept of the RESTORE technique is that it identifies and quantifies two components that are under-represented in CP spectra—one due to slow polarization transfer, the other due to rapid  $T_{1\rho}H$  relaxation—as well as one component that is easily seen by CP. Subspectra of the three identified components can be generated, and this gives information about the mechanisms that cause low CP observability and CP bias. The three RESTORE components are characterized by different values of  $T_{\text{CH}}$  and  $T_{1\rho}H$ .  $C_{\text{SS}}$  is characterized by rapid polarization transfer and rapid decay (short  $T_{\text{CH}}$  and short  $T_{1\rho}H$ ). It is under-represented in CP spectra due to its rapid rate of proton decay (short  $T_{1\rho}H$ ).  $C_{\text{SL}}$  is characterized by rapid polarization transfer and slow decay (short  $T_{\text{CH}}$  and long  $T_{1\rho}H$ ). It is easily detected by CP.  $C_{\text{LL}}$  is characterized by slow polarization transfer and slow decay (long  $T_{\text{CH}}$  and long  $T_{1\rho}H$ ). It is under-represented in CP spectra due to its slow rate of polarization transfer (long  $T_{\text{CH}}$ ).

The RESTORE subspectra for four of the kerogens are shown in Fig. 5. RESTORE was not possible for kerogen 4 on account of its extremely short  $T_{1\rho}H$  relaxation rate. RESTORE requires that there be few  $^{13}\text{C}$  nuclei characterized by both unfavourable  $T_{\text{CH}}$  and  $T_{1\rho}H$ , i.e. there is no component  $C_{\text{LS}}$  (long  $T_{\text{CH}}$  and short  $T_{1\rho}H$ ) in the analysis. This is not true for kerogen 4, for which most nuclei are characterized by very short  $T_{1\rho}H$ . For kerogen 5, no short  $T_{1\rho}H$  component was detected, and hence there are only two RESTORE components. Normal RESTORE analysis was therefore only possible for kerogens 1–3. Note that the RESTORE subspectra in Fig. 5 are scaled to reflect their

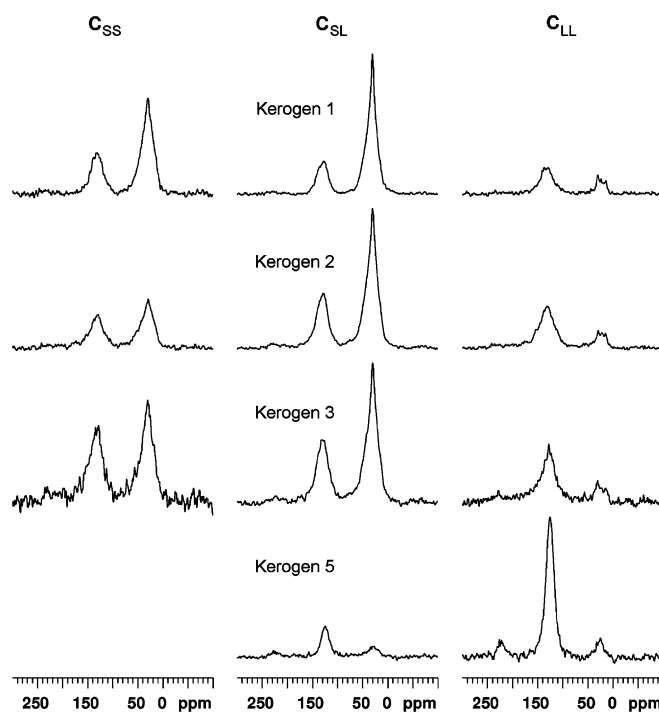


Fig. 5.  $^{13}\text{C}$  RESTORE subspectra of the kerogens.

relative contribution to the total RESTORE spectrum, i.e. their relative intensities should reflect the amount of carbon in each component.

For kerogens 1–3,  $C_{\text{SL}}$ , the most readily detected component, is the most abundant, followed by  $C_{\text{SS}}$  and  $C_{\text{LL}}$ . For each of these three kerogens,  $C_{\text{SL}}$  is the least aromatic component (Fig. 5, Table 6).  $C_{\text{SS}}$  is significantly more aromatic than  $C_{\text{SL}}$ . However, 34–52% of signal intensity for  $C_{\text{SS}}$  is in the aliphatic region (Table 6). It is this aliphatic C, characterized by rapid  $T_{1\rho}H$  relaxation, that is the aliphatic C “missing” from the normal (1-ms contact time)  $^{13}\text{C}$  CP spectra.  $C_{\text{LL}}$  is the most aromatic component (Fig. 5, Table 6). Note, also, the different shape of the alkyl resonances in the respective RESTORE subspectra (Fig. 5). For  $C_{\text{SL}}$ , there is a relatively sharp contribution, suggestive of long-chain alkyl structures; for  $C_{\text{SS}}$ , the alkyl peak is broader, suggesting shorter alkyl

Table 6  
Percentage of total signals assigned to three carbon types for RESTORE subspectra of the kerogens

	Carbonyl			Aromatic			Aliphatic		
	C <sub>SS</sub>	C <sub>SL</sub>	C <sub>LL</sub>	C <sub>SS</sub>	C <sub>SL</sub>	C <sub>LL</sub>	C <sub>SS</sub>	C <sub>SL</sub>	C <sub>LL</sub>
Kerogen 1	1.3	0.0	4.4	34.4	24.8	70.2	64.4	75.1	25.4
Kerogen 2	4.3	1.8	6.6	46.4	34.6	78.1	49.3	63.6	15.4
Kerogen 3	4.9	2.1	8.1	51.6	37.4	82.8	43.5	59.9	9.0
Kerogen 5		3.5	1.6		77.3	96.8		19.2	1.6

Table 7  
Best-fit values of  $T_{CH}$  and  $T_{1\rho}H$  for the three RESTORE components, specific observabilities of the components in a 1-ms contact time CP spectrum, and percent contribution of each component to total carbon

	C <sub>SS</sub>				C <sub>SL</sub>				C <sub>LL</sub>			
	$T_{CH}$ (ms)	$T_{1\rho}H$ (ms)	C <sub>obs,sp</sub>	%	$T_{CH}$ (ms)	$T_{1\rho}H$ (ms)	C <sub>obs,sp</sub>	%	$T_{CH}$ (ms)	$T_{1\rho}H$ (ms)	C <sub>obs,sp</sub>	%
Kerogen 1	0.2	0.68	0.315	42	0.2	3.01	0.761	49	5.00	3.01	0.153	9
Kerogen 2	0.2	0.72	0.334	29	0.2	3.59	0.794	57	3.85	3.59	0.199	14
Kerogen 3	0.2	0.50	0.216	40	0.2	2.60	0.730	50	5.00	2.60	0.150	10
Kerogen 5					0.2	4.00	0.813	36	5.00	4.00	0.160	64

chains; and for C<sub>LL</sub>, the small alkyl contribution has three peaks at around 30, 23 and 15 ppm. Given their chemical shift, these alkyl carbons must be protonated, so their slow rate of CP can only be explained by a high molecular mobility, and their three-peak structure suggests they are short, terminal groups, e.g. terminal methyl, ethyl or propyl groups. Short-chain alkyl groups with high molecular mobility have also been identified in kerogens using the dipolar dephasing technique [22].

The RESTORE subspectra for kerogen 5 are clearly very different, with C<sub>LL</sub> being by far the larger component. This shows that the aromatic structures in this kerogen are highly condensed, since all protonated carbons will appear in C<sub>SL</sub>, along with non-protonated carbons less than four bonds from a neighboring proton [52].

The results of the RESTORE fit are shown in Table 7. The  $T_{CH}$  value for C<sub>SS</sub> and C<sub>SL</sub> was fixed at 0.2 ms. The maximum value for  $T_{CH}$  in component C<sub>LL</sub> allowed in the fit (5 ms) was reached for three of the samples. C<sub>obs,sp</sub> is the specific observability of the component in a CP spectrum with a 1 ms contact time. It is a function of the component  $T_{CH}$  and  $T_{1\rho}H$  values. A low value of C<sub>obs,sp</sub> indicates a low observability for that component. The data in Table 7 confirm that C<sub>SL</sub> is the most observable component in a 1-ms contact time spectrum, and show that C<sub>SS</sub> and C<sub>LL</sub>, by comparison, produce 2–5 times less signal under standard CP conditions.

### 3.5. Replication of <sup>13</sup>C CP NMR spectra

In order to assess the degree of uncertainty in the determination of NMR spectral distributions, <sup>13</sup>C CP

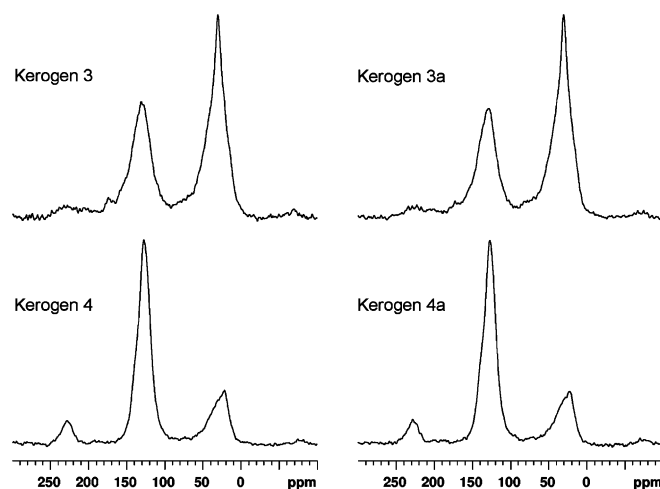


Fig. 6. Solid-state <sup>13</sup>C CP spectra of replicate samples of kerogens 3 and 4.

NMR spectra were acquired for replicate samples of kerogens 3 and 4. The replicate <sup>13</sup>C CP NMR spectra are shown in Fig. 6, and their chemical shift distributions are compared in Table 8. This comparison suggests that the precision of these measurements is about ±2% for aromatic and aliphatic carbon, and about ±0.5% for carbonyl carbon.

### 3.6. Spinning side bands

As discussed above, under the conditions that the spectra were run, there is a problem with the high-field (low ppm) aromatic SSB overlapping with the aliphatic central band.

Table 8  
Percentage of total signals assigned to three carbon types for  $^{13}\text{C}$  CP NMR spectra of replicate samples

	Carbonyl	Aromatic	Aliphatic
Kerogen 3	0.6	80.6	18.7
Kerogen 3a	0.9	82.4	16.7
Kerogen 4	3.6	45.2	51.2
Kerogen 4a	3.3	43.8	52.8

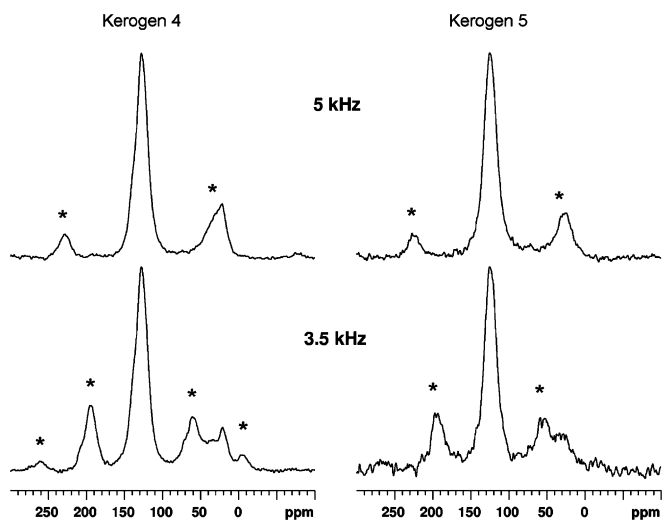


Fig. 7. Solid-state  $^{13}\text{C}$  CP spectra of kerogens 4 and 5 acquired at different rates of magic angle spinning. Spinning sidebands (SSBs) are marked with an asterisk (\*).

This problem is most acute for the thermally mature kerogens (4 and 5), since they consist primarily of aromatic C, and the aromatic SSB is of similar magnitude to the aliphatic central band. It was not possible to increase the MAS rate above the 5 kHz used, due to hardware limitations. Fig. 7 compares  $^{13}\text{C}$  CP spectra of kerogens 4 and 5 obtained at MAS rates of 5 and 3.5 kHz. The spectra obtained at the lower MAS rate clearly show that there is true aliphatic signal for both of these kerogens. The low MAS rate spectra also indicate that high- and low-field aromatic SSBs are of similar intensity, justifying our SSB corrections in the integral tables.

#### 4. Conclusions

Standard  $^{13}\text{C}$  CP NMR analysis of the kerogens in this study confirmed the well-established pattern of increasing aromaticity with increasing thermal maturity. However, the use of spin counting and RESTORE provided some fresh insights. Spin counting showed that the CP technique detected only around half of the potential signal for the immature kerogens, and this dropped to 14–25% for the mature kerogens. Spin counting also showed that the DP technique detected >80% of the potential signal for all but one of the kerogens. Despite the large differences in

observability between the two techniques, corresponding CP and DP spectra were not that different, although in all cases the DP spectra were more aromatic. There are two important points to take from these findings. The first is that the CP technique did provide a reasonably accurate measure of the chemistry of isolated kerogens. This is reassuring, given its widespread use for this purpose. The second is that great care must be taken when analyzing mixtures of kerogen and other types of organic matter, e.g. in studies probing the contribution of kerogen to the overall sorption properties of soil [7]. The low CP observability of kerogen means it will be under-represented in CP spectra relative to fresh organic matter, for which CP observabilities are usually much higher [27,45].

The RESTORE technique showed that the low CP observability of the immature kerogens could be attributed mostly to rapid  $T_{1\rho}H$  relaxation. Furthermore, this problem affected aliphatic as well as aromatic carbon, and thus accounted for most of the aliphatic C “missing” from the CP spectra.

Spin counting and RESTORE also showed that the two most thermally mature kerogens were actually quite different, despite the similar appearance of their  $^{13}\text{C}$  CP (and DP) spectra. The NMR observability of kerogen 4 was 30–45% higher than for kerogen 5 for both the CP and DP techniques. Furthermore, RESTORE indicated that the cause of low CP observability was quite different for these two kerogens. For kerogen 4, rapid  $T_{1\rho}H$  relaxation was the primary cause—this sample had the most rapid  $T_{1\rho}H$  relaxation rate. Conversely, kerogen 5 was characterized by the slowest rate of  $T_{1\rho}H$  relaxation, and its low CP observability could be attributed to slow polarization transfer, a consequence of a large proportion of its carbons being in highly condensed (graphitic) aromatic structures and hence far removed from nearest  $^1\text{H}$  neighbors.

#### Acknowledgments

We thank Bruno Kaegi (University of Zürich) for providing technical assistance.

#### References

- [1] B. Tissot, D.H. Welte, *Petroleum Formation and Occurrence*, Springer, Berlin, 1978.
- [2] J.I. Hedges, J.M. Oades, *Org. Geochem.* 27 (1997) 319.
- [3] S.T. Petsch, R.A. Berner, *Am. J. Sci.* 298 (1998) 246.
- [4] W. Huang, W.J. Weber Jr., *Environ. Sci. Technol.* 31 (1997) 2562.
- [5] M.D. Johnson, T.M. Keinath III, W.J. Weber Jr., *Environ. Sci. Technol.* 35 (2001) 1688.
- [6] M.D. Johnson, W. Huang, W.J. Weber Jr., *Environ. Sci. Technol.* 35 (2001) 1680.
- [7] J. Song, P. Peng, W. Huang, *Environ. Sci. Technol.* 36 (2002) 3960.
- [8] Y. Ran, B. Xiao, W. Huang, P. Peng, D. Liu, J. Fu, G. Sheng, *J. Environ. Qual.* 32 (2003) 1701.
- [9] R.L. Patience, A.L. Mann, I.J.F. Popplett, *Geochim. Cosmochim. Acta* 56 (1992) 2725.
- [10] U. Werner-Zwanziger, G. Lis, M. Mastalerz, A. Schimmelmann, *Solid State Nucl. Magn. Reson.* 27 (2005) 140.

- [11] L.W. Dennis, G.E. Maciel, P.G. Hatcher, B.R.T. Simoneit, *Geochim. Cosmochim. Acta* 46 (1982) 901.
- [12] F.P. Mikinis, D.A. Netzel, J.W. Smith, M.A. Mast, G.E. Maciel, *Geochim. Cosmochim. Acta* 46 (1982) 977.
- [13] A.J.G. Barwise, A.L. Mann, G. Eglinton, A.P. Gowar, A.M.K. Wardroper, C.S. Gutteridge, *Org. Geochem.* 6 (1984) 343.
- [14] M.J. Trewthella, I.J.F. Poplett, A. Grint, *Fuel* 65 (1986) 541.
- [15] M.A. Wilson, *NMR Techniques and Applications in Geochemistry and Soil Chemistry*, Pergamon Press, Oxford, 1987 (pp. 62–94).
- [16] E.G. Witte, H.J. Schenk, P.J. Muller, K. Schwochau, *Adv. Org. Geochem.* 13 (1987) 1039.
- [17] A.L. Mann, R.L. Patience, I.J.F. Poplett, *Geochim. Cosmochim. Acta* 55 (1991) 2259.
- [18] S. Bharati, R.L. Patience, S.R. Larter, G. Standen, J.F. Poplett, *Org. Geochem.* 23 (1995) 1043.
- [19] Z. Zujovic, R. Srejec, D. Vucelic, D. Vitorovic, B. Jovancicevic, *Fuel* 74 (1995) 1903.
- [20] T. Mongenot, S. Derenne, C. Largeau, N.-P. Tribouvillard, E. Lallier-Verges, D. Dessort, J. Connan, *Org. Geochem.* 30 (1999) 39.
- [21] F.J. Gonzalez-Vila, A. Ambles, J.C. del Rio, L. Grasset, *J. Anal. Appl. Pyrol.* 58–59 (2001) 315.
- [22] S.T. Petsch, R.J. Smernik, T.I. Eglinton, J.M. Oades, *Geochim. Cosmochim. Acta* 65 (2001) 1867.
- [23] U. Lille, I. Heinmaa, T. Pehk, *Fuel* 82 (2003) 799.
- [24] Z. Wei, X. Gao, D. Zhang, J. Da, *Energy Fuels* 19 (2005) 240.
- [25] C.E. Snape, D.E. Axelson, R.E. Botto, J.J. Delpuech, P. Tekely, B.C. Gerstein, M. Pruski, G.E. Maciel, M.A. Wilson, *Fuel* 68 (1989) 547.
- [26] A. Jurkiewicz, G.E. Maciel, *Anal. Chem.* 67 (1995) 2188.
- [27] R.J. Smernik, J.M. Oades, *Geoderma* 96 (2000) 159.
- [28] R.J. Smernik, *Geoderma* 125 (2005) 249.
- [29] C.J. Golding, R.J. Smernik, G.F. Birch, *Environ. Sci. Technol.* 39 (2005) 3925.
- [30] E.W. Hagaman, R.R. Chambers Jr., M.C. Woody, *Anal. Chem.* 58 (1986) 387.
- [31] J.V. Muntean, L.M. Stock, R.E. Botto, *Energy Fuels* 2 (1988) 108.
- [32] G.D. Love, R.V. Law, C.E. Snape, *Energy Fuels* 7 (1993) 639.
- [33] S. Wiggershaus-Eschert, I. Wieschenkammer, W. Riepe, Fresenius *J. Anal. Chem.* 346 (1993) 805.
- [34] A. Jurkiewicz, G.E. Maciel, *Fuel* 73 (1994) 829.
- [35] M.M. Maroto-Valer, C.J. Atkinson, R.R. Willmers, C.E. Snape, *Energy Fuels* 12 (1998) 833.
- [36] R.J. Smernik, J.M. Oades, *Eur. J. Soil Sci.* 54 (2003) 103.
- [37] L. Schwark, A. Frimmel, *Chem. Geol.* 206 (2004) 231.
- [38] L. Schwark, W. Püttmann, *Org. Geochem.* 16 (1990) 749.
- [39] M. Vliex, L. Schwark, D. Leythaeuser, *Z. Geol. Paläontol.* I (1999) 1447.
- [40] K. Scheffler, S. Hoernes, L. Schwark, *Z. Geol. Paläontol.* I (2001) 155.
- [41] L. Schwark, M. Vliex, P. Schaeffer, *Org. Geochem.* 29 (1998) 1921.
- [42] J. Espitalié, J.L. Laporte, M. Madec, F. Marquis, P. Leplat, J. Paulet, A. Boutefeu, *Rev. Inst. Français Pétrole* 32 (1977) 23.
- [43] M.L. Bordenave, J. Espitalié, P. Leplat, J.L. Oudin, M. Vandembroucke, Screening techniques for source rock evaluation, in: M.L. Bordenave (Ed.), *Applied Petroleum Geochemistry*, Éditions Technip, Paris, 1993, pp. 219–278.
- [44] R.J. Smernik, J.M. Oades, *Solid State Nucl. Magn. Reson.* 20 (2001) 74.
- [45] R.J. Smernik, J.M. Oades, *Geoderma* 96 (2000) 101.
- [46] R.J. Smernik, J.A. Baldock, J.M. Oades, A.K. Whittaker, *Solid State Nucl. Magn. Reson.* 22 (2002) 50.
- [47] W. Küspert, Environmental changes during oil-shale deposition as deduced from stable isotope ratios, in: G. Einsele, A. Seilacher (Eds.), *Cyclic and Event Stratification*, Springer, Berlin, 1982, pp. 482–501.
- [48] J.M. Moldowan, P. Sundararaman, M. Schoell, *Org. Geochem.* 10 (1986) 915.
- [49] S. Schouten, H.M.E. van Kaam-Peters, W.I.C. Rijpstra, M. Schoell, J.S. Sinninghe Damsté, *Am. J. Sci.* 300 (2000) 1.
- [50] H.-J. Röhl, A. Schmid-Röhl, W. Oschmann, A. Frimmel, L. Schwark, *Palaeogeogr. Palaeoclim. Palaeoecol.* 165 (2001) 27.
- [51] A. Frimmel, W. Oschmann, L. Schwark, *Chem. Geol.* 206 (2004) 199.
- [52] L.B. Alemany, D.M. Grant, R.J. Pugmire, T.D. Alger, K.W. Zilm, *J. Am. Chem. Soc.* 105 (1983) 2142.